

1 **Characterizing grapevine (*Vitis* spp.) inflorescence architecture using X-** 2 **ray imaging: implications for understanding cluster density**

3
4 Mao Li¹, Laura L. Klein^{1,2}, Keith E. Duncan¹, Ni Jiang¹, Jason P. Londo³, Allison J. Miller^{1,2},
5 Christopher N. Topp^{1,*}

6
7 ¹Donald Danforth Plant Science Center, 975 North Warson Road, St. Louis, MO 63132-2918, USA

8 ²Department of Biology, Saint Louis University, 3507 Laclede Avenue, St. Louis, MO 63103-2010, USA

9 ³United States Department of Agriculture, Agricultural Research Service: Grape Genetics Research Unit, 630
10 West North Street, Geneva, NY 14456-1371, USA

11
12 *Corresponding author:

13 Christopher N. Topp

14 Donald Danforth Plant Science Center, 975 North Warson Road, St. Louis, MO 63132-2918, USA

15 Tel.: (314) 587-1609

16 Email: ctopp@danforthcenter.org

17 18 19 **Summary**

20
21 We characterized grapevine inflorescence architecture (the rachis and all branches
22 without berries) to describe variation among 10 wild *Vitis* species, assess phylogenetic
23 signals underlying inflorescence architecture traits, and interpret this variation in the
24 context of breeding objectives.

25 Three-dimensional X-ray tomography scans of grapevine inflorescences were used
26 to measure geometric traits and inflorescence topology using persistent homology, a
27 mathematical approach that can comprehensively measure and compare shapes. We
28 simulated potential space available for berry growth within a given inflorescence
29 architecture by evaluating expanding spheres attached to pedicels, referred to as “berry
30 potential.” Lastly, we performed phylogenetic analysis and mapped trait variation.

31 We detected wide variation in inflorescence architecture features among *Vitis*
32 species. Hierarchical clustering and correlation analyses revealed relationships among
33 traits. Multivariate analyses identify traits contributing the most to variation and
34 distinguish between species with high accuracy. Phylogenetic analyses revealed 12
35 morphological traits with strong phylogenetic signal.

36 Morphometric analysis uncovered novel differences in inflorescence architecture
37 among clades and between *Vitis* species. Cluster density is an important trait for assessing
38 crop quality and forecasting yield; analyses presented here can be used to tease apart
39 subtle, heritable features and environmental influences on this major agronomic trait.

40
41 Key words: berry potential; inflorescence; morphology; persistent homology; phylogenetic
42 analysis; topological data analysis; *Vitis* spp.; X-ray tomography

43 44 **Introduction**

45
46 Inflorescences are major adaptations of the angiosperm lineage whose architectural
47 variation affects fertilization, fruit development, dispersal, and crop yield (Wyatt, 1982;

48 Hake, 2008; de Ribou *et al.*, 2013; Kirchoff & Claßen-Bockhoff, 2013; Périlleux *et al.*, 2014;
49 Chanderbali *et al.*, 2016). These branched reproductive structures with multiple flowers
50 reflect the extraordinary diversity across angiosperm species, from an ear of corn to palms
51 with inflorescences measuring five meters long (Hodel *et al.*, 2015). Yet seemingly simple
52 processes give rise to these vastly different shapes - during development reproductive
53 meristems may either switch to floral identity or proliferate additional inflorescence
54 meristems and branches (Prusinkiewicz *et al.*, 2007). Complex topologies reflect the
55 evolution of this functional diversity, but have proven difficult to quantify with
56 conventional tools.

57
58 Detailed descriptions of inflorescences by trained experts are often unique to specific
59 research communities or groups of taxa, and are not always readily transferable, hindering
60 meaningful comparative analysis (Endress, 2010). Inflorescences are sometimes described
61 typologically: indeterminate or determinate, simple or compound, as a raceme, cyme,
62 panicle or spike, etc. (Wyatt, 1982; Weberling, 1992). Other approaches describe
63 qualitative attributes of inflorescences such as the presence or absence of certain
64 structures (Weberling, 1992; Doebley *et al.*, 1997; Feng *et al.*, 2011; Hertweck & Pires,
65 2014). A third method for characterizing inflorescences is through quantification of
66 component structures (e.g., branch length, inflorescence length and width, angular traits;
67 Kuijt, 1981; Marguerit *et al.*, 2009; Landrein *et al.*, 2012; Le *et al.*, 2018). Although these
68 classical quantitative approaches facilitate comparative statistical analyses, the three-
69 dimensional (3D) complexity of inflorescences is largely undescribed. Furthermore,
70 descriptions may be confounded by developmental stage at the time of measurement, and
71 distinguishing between vegetative and reproductive branching structures can be difficult
72 (Wyatt, 1982; Weberling, 1992; Guédon *et al.*, 2001). Thus, new technological and
73 analytical approaches that can represent comprehensive, multi-dimensional information
74 about inflorescence diversity are needed to normalize and enrich analysis of these
75 structures.

76
77 One promising approach for capturing 3D shapes of inflorescences and other plant
78 structures is X-ray tomography (XRT). XRT generates high quality reconstructions of the
79 internal and external shapes of plants, preserving nearly complete geometric and
80 topological information in 3D. These 3D digital models then can be used to extract
81 quantitative data (features) from plant structures. X-rays have been used to quantify wheat
82 and rice seed and inflorescence traits from intact samples for non-destructive yield
83 calculations (Hughes *et al.*, 2017; Jhala & Thaker, 2015), internal anatomy of willow trees
84 (Brereton *et al.*, 2015), stem morphology and anatomy in sorghum (Gomez *et al.*, 2018),
85 root structure of barley seedlings (Pfeifer *et al.*, 2015), leaf anatomy in monocots and dicots
86 (Mathers *et al.*, 2018) and dynamic starch accumulation in living grapevine stems (Earles *et al.*,
87 2018), among others. Most critically, whereas manual measurements can be laborious
88 and destructive, non-destructive sampling for XRT analysis facilitates comprehensive
89 quantification of complex morphological traits.

90
91 Quantifying complex shapes with XRT requires appropriate analytical approaches.
92 Topological modeling, a mathematical field concerned with the connectedness of branching
93 structures, can quantify inflorescence architecture by parsing geometric 3D structures into

94 distinct, yet connected, components (Godin & Caraglio, 1998). Topological modeling has
95 yielded important insights into inflorescence development, functional analysis, and crop
96 improvement in a variety of plant species (e.g., *Arabidopsis thaliana*, *Capsicum annuum*,
97 *Malus pumila*, and *Triticum*; Godin *et al.*, 1999; Letort *et al.*, 2006; Kang *et al.*, 2009). While
98 powerful, these reductionist approaches rely on an a priori understanding of the
99 mechanisms that contribute to complexity (e.g., branching patterns), and lose power when
100 shapes vary drastically from one another (e.g., comparing a corn tassel to a grape cluster).
101 Approaches that capture emergent properties of complex structures without presupposing
102 the importance of individual structural components are complementary to traditional
103 topological models (Bucksch *et al.*, 2017).

104
105 An emerging mathematical approach to interpret topological models is persistent
106 homology (PH). PH extracts morphological features from two- or three-dimensional
107 representations and can be used to compare very different shapes. PH has been applied to
108 explain a wide range of features including atomic structures, urban and forested areas,
109 cancers, cell shapes, and jaw shape, among others (Edelsbrunner & Morozov, 2013). In
110 plants, PH has been used to estimate shapes that are otherwise difficult to measure
111 including leaves, leaflet serration, spikelet shape, stomatal patterning, and root
112 architecture (Li *et al.*, 2018a,b; Haus *et al.*, 2018; McAllister *et al.*, 2019; Migicovsky *et al.*
113 2018). Previous work showed that PH could capture more quantitative variation than
114 traditional plant morphological measures (described above) resulting in the identification
115 of otherwise latent quantitative trait loci (Li *et al.*, 2018b). PH is especially well-suited for
116 quantifying branching topology as it can quantitatively summarize complex variation with
117 a single measure (Li *et al.*, 2017; Delory *et al.*, 2018). Rachis, pedicel, and branches include
118 inherently topological features that can be especially well-analyzed with PH-based
119 methods.

120
121 Grape clusters (or bunches) are branched structures supporting berries produced by
122 grapevines (*Vitis* spp.) and are an ideal system in which to apply XRT and PH. Grape
123 infructescences are historically, culturally, and economically important and vary
124 extensively in nature and in cultivation (Iland *et al.*, 2011). Cluster architecture determines
125 bunch density, and is defined as “arrangement of berries in a cluster and the distribution of
126 free space” (Richter *et al.*, 2018). The density of berries in a cluster is an important
127 breeding feature because it determines yield, wine character, and disease resistance
128 (amount of air flow between berries is a primary determinant of pests and pathogens on
129 the fruit). Cluster density is a characteristic identified by the Organization Internationale de
130 la Vigne et du Vin, and varies from “berries clearly separated” (loose clusters) to “berries
131 deformed by compression” (very dense clusters; OIV, 2001). As one of the primary
132 determinants of yield, end-product characteristics, and disease resistance cluster
133 architecture has been studied extensively in grapevine (reviewed in Tello & Ibáñez, 2018).
134 These studies have shown that wine grape cultivars (*Vitis vinifera*) display distinct bunch
135 densities (Shavrukov *et al.*, 2004). However, less is known about cluster architecture in
136 wild *Vitis* species, an important source of natural variation used by breeders in the
137 development of hybrid grapevine varieties.

138

139 Historically, researchers have focused on a suite of cluster traits such as cluster size, shape,
140 weight, and density/compactness to characterize bunch density quantified in grapevines
141 (Rovasenda, 1881; Pulliat, 1888; Bioletti, 1938; Galet, 1979; Bettiga, 2003). Measurements
142 are made primarily using traditional tools including rulers, digital calipers, volume
143 displacement, and/or through human judging panels. More recently, automated image-
144 based approaches have been implemented to capture aspects of cluster architecture in the
145 lab and field (Ivorra *et al.*, 2015; Aquino *et al.*, 2017, 2018; Rist *et al.*, 2018). However, these
146 image-based methods cannot penetrate the internal inflorescence structure. Therefore
147 resulting models are based only the visible surface and the underlying topology cannot be
148 fully captured, limiting an understanding of how inflorescence architecture and berry
149 features co-vary. XRT and PH applications offer an important opportunity to understand
150 grapevine bunch density through detailed analyses of inflorescence architecture. This work
151 will deepen our understanding of natural variation of inflorescence structure, identify
152 priority targets for breeding, and permit connecting 3D structure to underlying processes
153 and genetics of inflorescence development.

154
155 We use X-ray tomography, geometric measurements, persistent homology, and
156 computational simulation to characterize wild grapevine inflorescence architecture. We
157 target the branching architecture of the mature inflorescence: the rachis and all branches
158 that remain following the removal of ripe berries (Fig. 1). Specifically, we aim to: 1)
159 characterize variation in component traits of inflorescence architecture within and among
160 *Vitis* species; 2) assess phylogenetic signals underlying inflorescence architecture traits;
161 and 3) interpret inflorescence trait variation in the context of breeding objectives. This
162 work represents an important advance for the characterization of 3D plant architecture
163 using a powerful combined imaging and computational approach.

164

165 **Materials and Methods**

166

167 **Plant Material**

168

169 In this study, we sampled grapevine bunches from 136 unique genotypes representing 10
170 wild *Vitis* species living in the USDA germplasm repository system (Geneva, NY; Table 1,
171 Fig. S1). Grapevines have a paniculate inflorescence that consists of a rachis with several
172 primary and secondary branches, tapering towards the terminus of the organ (Iland *et al.*,
173 2011). Wild grapevines are dioecious; consequently, unbalanced sample sizes for different
174 species reflect numbers of female genotypes available in the germplasm collection. Each
175 unique genotype is represented in the germplasm collection by two clonally replicated
176 vines. For most of the 136 genotypes, we collected a total of three clusters from the two
177 clonal replicates combined, representing average cluster morphology. We avoided clusters
178 that were visibly damaged or indirectly altered (e.g., tendril or trellis interference). For
179 each vine, clusters were removed from separate canes at the point of peduncle attachment
180 (Fig. 1a). In total, 392 clusters were collected in September 2016 when berries were soft,
181 equivalent to EL38 developmental stage (Coombe, 1995; Fig. 1b). Berries were manually
182 removed from clusters in the field, and the remaining inflorescence stalks (including rachis,

183 branches, and pedicels; hereafter referred to as inflorescence or inflorescence architecture)
184 were used to assess inflorescence architecture.

185

186 **X-ray tomography and data preprocessing**

187

188 Grapevine inflorescences were scanned at the Donald Danforth Plant Science Center (St.
189 Louis, MO) using a North Star Imaging X5000 X-ray tomography instrument (NSI; Rogers,
190 MN) equipped with a 16-bit Varian flat panel detector (1536 x 1920 pixels with 127um
191 pixel pitch) and 225kV microfocus reflection target X-ray source. Each inflorescence was
192 held between two pieces of construction-grade expanded polystyrene, clamped in a
193 panavise, and positioned on the X-ray turntable in one of two configurations (Fig. 1c):
194 725mm from the source, generating 1.26x magnification and 101um voxel resolution, or
195 766mm from the source, generating 1.19x magnification and 107um voxel resolution. Each
196 scan used X-ray wattage set to 60kV and 1200uA at 10 frames per second, collecting 1200
197 16-bit TIFF projections over 360 degrees of rotation during a 2min continuous standard
198 scan. Projections for each scan (Fig. 1d) were combined into a single 3D volume using NSI
199 efX-CT software, converted to a density-based surface rendering Polygon file (PLY), and
200 exported for analysis (Fig. 1e). The full PLY data set for this work is 7.85GB, and can be
201 downloaded from: [https://www.danforthcenter.org/scientists-research/principal-](https://www.danforthcenter.org/scientists-research/principal-investigators/chris-topp/resources)
202 [investigators/chris-topp/resources](https://www.danforthcenter.org/scientists-research/principal-investigators/chris-topp/resources).

203

204 We exported the surface mesh data (.ply files) into Meshlab (v1.3.3, (Cignoni *et al.*, 2008)
205 and performed the following processing steps to remove topological noise: 1) deleted the
206 vertices where branches touch using “Select Vertexes” and “Delete Selected vertices” filters;
207 2) removed duplicates and isolated vertices and faces using the filters “Remove Duplicated
208 Vertex,” “Remove Duplicate Faces,” “Remove Isolated pieces (wrt Diameter),” and “Remove
209 Unreferenced Vertex.”

210

211 **Geometric inflorescence architecture traits**

212

213 We extracted 15 geometric traits from scanned inflorescences (Fig. 2, Fig. S2). Detailed trait
214 descriptions and calculations are explained in Table S1. Trait illustrations, including
215 examples of low and high values for each trait, are available in Fig. 2 and Fig. S2. Traits
216 were organized in one of three trait groups: global-size features, local-branching features,
217 and size-invariant features (Table 2). PedicelDiameter and PedicelBranchAngle were
218 measured using the software DynamicRoots (Symonova et al. 2015) on a subset of detected
219 pedicels from the raw 3D volume data. All other traits were derived from Matlab
220 algorithms. Branch length traits (i.e., TotalBranchLength, RachisLength, PedicelLength, and
221 AvgBranchLength) were derived from the persistence barcode (see next subsection).

222

223 **Quantifying branching topology using persistent homology, a topological data** 224 **analysis method**

225

226 Persistent homology measures shapes based on a tailored mathematical function, such as
227 geodesic distance, which we used here to capture both curved length and topology of the
228 branches (Fig. 3, Video S1). The geodesic distance of a point is the length of the shortest

229 curve connecting the point and the base (e.g. purple curves, Fig. 3a), where the tailored
230 base can be set as the first node or ground level (the brown line in Fig. 3a). For each branch,
231 the tip always has the largest geodesic distance from the base (Fig. 3b). A level represents
232 the collection of points whose geodesic distances are the same (e.g. geodesic distance=90,
233 pink curve in Fig. 3a). A superlevel set, for example, at 90, is all the points whose geodesic
234 distances are greater than 90 (black branch tips, Fig. 3a). Changing the level value from
235 largest to smallest (x axis, Fig. 3c), the sequence of nesting superlevel sets can be formed,
236 which is named superlevel set filtration (top panel, Fig. 3c). During the change of the level
237 value, bars record the connected components for each of the superlevel sets. When a new
238 component arises, a new bar starts (e.g. at level 112, purple branch, Fig. 3c). When two
239 components merge (e.g. at level 65, orange branch merges into purple branch, Fig. 3c), the
240 shorter bar stops (e.g. the orange bar stops at level 65, Fig. 3c). This bar graph, called the
241 persistence barcode, summarizes topological information such as branching hierarchy,
242 branch arrangement, and branch lengths. In our study, we set the base as the junction
243 between peduncle and rachis (the lowermost node, indicated by a brown line in Fig. 1e, Fig.
244 3d, f) and use this base to compute the persistence barcode for the inflorescence
245 architecture (Fig. 3e, g).

246
247 The persistence barcode can be used to compare topological similarity between any two
248 inflorescences. To compute pairwise distance among persistence barcodes for the entire
249 inflorescence population, we used the bottleneck distance (Cohen-Steiner *et al.*, 2007).
250 Bottleneck distance is a robust metric that calculates the minimal cost to move bars from
251 one persistence barcode to resemble another (Li *et al.*, 2017). We performed
252 multidimensional scaling (MDS) on the pairwise bottleneck distance matrix and projected
253 the data into lower dimensional Euclidean space by preserving the pairwise distance as
254 well as possible. The Matlab (R2017a) MDS function `cmdscale()` projects the data so that
255 MD1 acts as PC1 representing the most variation. The first three PCs (MDs) explained
256 about 80% of the total variation and were included as traits: PersistentHomology_PC1
257 (PH_PC1, explained about 54% variation), PersistentHomology_PC2 (PH_PC2, explained
258 about 20% variation), and PersistentHomology_PC3 (PH_PC3, explained about 6%
259 variation). Those traits not only measure the topological structure, but also relate to
260 geometric variation (e.g. global size) as the data were not normalized (Fig. 2, Table S1).

261
262 Next, we normalized the persistence barcode by the TotalBranchLength (summation of the
263 bar lengths) so that the TotalBranchLength was 1. By a similar procedure, we derived the
264 first three PCs named PersistentHomologyNormalizedByTotalBranchLength_PC1
265 (PHn_PC1, explained about 45% variation),
266 PersistentHomologyNormalizedByTotalBranchLength_PC2, (PHn_PC2, explained about
267 21% variation), and PersistentHomologyNormalizedByTotalBranchLength_PC3 (PHn_PC3,
268 explained about 7% variation) for the normalized inflorescence topological structure (Fig.
269 2, Table S1).

270
271 **Berry potential, an approach to indirectly explore the space limited by inflorescence**
272 **architecture**

273

274 An ongoing question in grapevine cluster architecture is the relationship between
275 inflorescence architecture and berry number and size. Inflorescence architecture is one of
276 several factors determining the number of berries that can form, due to the number of
277 pedicels and the available space for berry development. In this study, berries were
278 removed because of concerns about berry integrity during transport from New York to
279 Missouri, and the time between harvest and scanning. Instead of looking directly at berries
280 on the cluster, we used inflorescence architecture as a starting point to simulate potential
281 space available for berry growth by evaluating expanding spheres attached to pedicels. The
282 extent of sphere expansion allowed by each pedicel is referred to as “berry potential” (Fig.
283 4, Video S2).

284
285 We first determined the growth direction for each berry potential based on the pedicel
286 orientation. When spheres expand, the center moves along the pedicel direction (Fig. 4a).
287 This step can be achieved by performing principal component analysis (PCA) on the near-
288 berry segment of the pedicel. The first principal axis is the pedicel direction. We adjusted
289 the arrow of the direction to make sure berry potential increases outward along the pedicel
290 orientation. Then the berry potential increases until one of three situations is encountered
291 (Fig. 4b): 1) if two berry potentials touch to each other, both berry potentials will stop
292 increasing; 2) if a berry potential touches any part of the inflorescence, it will stop
293 increasing; 3) if the diameter of the berry potential reaches the maximum size known for
294 that species (Table 1), it will stop increasing. For each species, the maximum size is defined
295 as the maximum berry diameter, a number estimated from known ranges of berry sizes for
296 each species, based on values obtained from (Galet, 1988; Moore & Wen, 2016).

297
298 Berry potential does not reflect true berry growth; rather, berry potential is a derived
299 attribute of inflorescence architecture, an indirect estimate of the space potentially
300 available for berry growth. It also does not account for the possibility of branches bending
301 or otherwise becoming re-oriented due to pressure from growing berries. Berry potential
302 is based on the number of neighbor pedicels, neighbor pedicel lengths, and neighbor
303 pedicel mutual angles. Larger values for berry potential are associated with fewer neighbor
304 pedicels, and/or longer pedicel lengths, and/or larger mutual angles. From the berry
305 potential simulation, we calculated three features, TotalBerryPotentialVolume,
306 AvgBerryPotentialDiameter, and BerryPotentialTouchingDensity, which is the berry
307 potential touching number (i.e., touching either another berry potential or any part of the
308 inflorescence) divided by the number of berry potential (Fig. 2, Table S1).

309 310 **Phylogenetic analysis**

311
312 Phylogenetic analyses were conducted to understand evolutionary trends in inflorescence
313 architecture in *Vitis*. Single nucleotide polymorphism (SNP) markers were generated as
314 part of a separate study of the USDA Grapevine Germplasm Reserve in Geneva, NY (Klein *et al.*,
315 2018). The original dataset consisted of 304 individuals representing 19 species that
316 were sequenced using genotyping-by-sequencing (GBS; Elshire *et al.*, 2011). Briefly, Klein
317 *et al.* (2018) filtered data to retain biallelic sites with a minimum allele frequency of 0.01, a
318 minimum mean depth of coverage of 10x, and only sites with <20% missing data and
319 individuals with <20% missing data. SNP data for 99 individuals from this study that were

320 also genotyped in (Klein *et al.*, 2018); Table 1) were extracted using custom scripts. We
321 performed phylogenetic analysis on the sequence data extracted for 99 individuals using
322 SVDquartets (Chifman & Kubatko, 2014), a maximum likelihood approach designed to
323 address ascertainment bias associated with reduced representation sequencing techniques
324 like GBS. We analyzed all possible quartets and carried out 100 bootstrap support runs
325 (Fig. S1) using PAUP* version 4.0a (Swofford, 2003). The three main clades recovered in
326 the tree were consistent with previous phylogenetic work in *Vitis*: 1) an Asian Clade (*V.*
327 *amurensis* and *V. coignetiae*), 2) North American Clade I (*V. riparia*, *V. acerifolia*, and *V.*
328 *rupestris*), and 3) North American Clade II (*V. vulpina*, *V. cinerea*, *V. aestivalis*, *V. labrusca*,
329 and *V. palmata*) (Tröndle *et al.*, 2010; Zecca *et al.*, 2012; Miller *et al.*, 2013; Zhang *et al.*,
330 2015; Klein *et al.*, 2018).

331
332 To visualize trait distributions on a phylogenetic tree using branch lengths, we used Mega X
333 (Kumar *et al.*, 2018) to generate a neighbor joining tree with 2000 bootstrap replicates. All
334 measurements were averaged across the three replicates per genotype to produce an
335 average value for each trait for each genotype. We computed Pagel's lambda to estimate
336 phylogenetic signal for each morphological trait and mapped each trait onto the phylogeny
337 (Fig. S3a-x) using the R package phytools (v. 0.6-44; Revell, 2012). We calculated variation
338 of each morphological trait for each clade based on the mean value for each species (Fig.
339 S4).

340 341 **Statistical analysis**

342
343 PCA, MDS, and hierarchical cluster analysis generating a hierarchical tree were performed
344 in Matlab using functions `pca()`, `cmdscale()`, and `clustergram()`. The R function `cor.mtest()`
345 and package `corrplot` (Wei & Simko, 2017) were used for significance tests and correlation
346 matrix visualization. The function `lda()` in R package MASS (Venables & Ripley, 2002) was
347 used for the linear discriminant analysis (LDA) with a jackknifed 'leave one out' cross
348 validation method.

349 350 **Code availability**

351
352 All Matlab functions used to calculate persistence barcodes, bottleneck distances,
353 simulation for berry potential, other geometric features used in this study, and the script
354 for extracting phylogenetic information can be found at the following GitHub repository:
355 <https://github.com/Topp-Roots-Lab/Grapevine-inflorescence-architecture>.

356 357 **Results**

358 359 **Inflorescence morphological variation and trait correlation within *Vitis* species**

360
361 We investigated 24 morphological traits (15 geometric traits, six PH traits, and three berry
362 potential traits) of inflorescence architecture in 10 wild *Vitis* species (136 genotypes, 392
363 samples) and detected wide variation in morphological features within and between
364 species (Fig. 2, Fig. S2, and Table S2). In particular, of all the species examined, *V. aestivalis*

365 has the largest variance for TotalBerryPotentialVolume. *V. labrusca* has the largest variance
366 for ten traits (i.e., pedicel features, Sphericity, AvgBranchDiameter,
367 AvgBerryPotentialDiameter, and normalized topological traits). *V. cinerea* has the largest
368 variance for six traits (i.e., most global-size features, PH_PC2, and PH_PC3). In comparison,
369 *V. palmata* has smallest variance for eight traits (i.e. pedicel features, Sphericity,
370 AvgBranchDiameter, TotalBerryPotentialVolume, PH_PC3, and PHn_PC3), as does *V.*
371 *amurensis* (global-size features, RachisLength, PH_PC1, and PH_PC2).

372
373 All traits were hierarchically clustered based on the mean trait values for each species,
374 classifying traits into two main categories: mostly size-invariant + local-branching features
375 (PHn_PC3 to PedicelLength), versus global-size features (AvgBranchLength to
376 BerryPotentialTouchingDensity) (Fig. 5a). Hierarchical clustering (Fig. 5a) and pairwise
377 correlation for morphological traits (Fig. 5b) show that global-size features
378 (ConvexHullVolume, SurfaceArea, Volume, NumberOfPedicel, and TotalBranchLength),
379 PH_PC1, and RachisLength are all highly positively correlated. We refer to these seven
380 traits as size-associated features. Size-associated features are negatively correlated with
381 PedicelLength/RachisLength, Solidity, Sphericity, and PHn_PC1. Some traits are relatively
382 independent such as 2nd/LongestBranchLength, PedicelLength, PedicelBranchAngle,
383 PH_PC2, PHn_PC2, and PHn_PC3 (Fig. 5b). PH_PC3 has some negative relation with size-
384 invariant features. PHn_PC1 positively correlates with Sphericity, Solidity, and
385 AvgBerryPotentialDiameter (Fig. 5b). Pairwise correlations of morphological features
386 (allometric relationships) for each of the species vary widely (Fig. 5c; for all traits see Fig.
387 S5a-x). For example, more pedicels typically result in smaller berry potential diameters,
388 except for *V. aestivalis*. Longer branches tend to be thinner, except for *V. coignetiae*, and
389 correlate with larger inflorescences, except in *V. acerifolia*.

390
391 Hierarchical clustering of 10 *Vitis* species based on the 24 morphological traits resolved
392 four groups: 1) *V. cinerea*, 2) *V. aestivalis*, 3) *V. coignetiae*/*V. vulpina*/*V. palmata*/*V.*
393 *acerifolia*/*V. riparia*/*V. rupestris*, and 4) *V. amurensis*/*V. labrusca* (Fig. 5a). Among the 10
394 *Vitis* species examined in this study, the largest variance in mean trait values are seen in *V.*
395 *cinerea* (Fig. 5a). *V. cinerea* samples are generally larger than those from the other species,
396 as reflected in size-associated traits. Topology traits such as PHn_PC3 and size-invariant
397 traits like Sphericity and Solidity are lower in the mean trait value for *V. cinerea* than for
398 other species. Similarly, mean trait values are larger for size-associated traits in *V. aestivalis*
399 (Fig. 5a). Compared to other species, topology and berry potential traits are larger in *V.*
400 *aestivalis*. Mean trait values of the third group (*V. coignetiae*/*V. vulpina*/*V. palmata*/*V.*
401 *acerifolia*/*V. riparia*/*V. rupestris*, Fig. 5a) tend to be nearer to middle values compared to
402 the other species. Within this group, *V. acerifolia*/*V. riparia*/*V. rupestris* typically are larger
403 in the mean trait value for berry potential touching (i.e., denser berry potentials). These
404 three species and *V. palmata* tend to have large, first primary branches (i.e., wings; Fig. 1e).
405 *V. coignetiae* has thicker branches and *V. vulpina* has longer pedicels compared to other
406 species in this group. The final group, *V. amurensis* and *V. labrusca*, have relatively smaller
407 inflorescences with thicker branches compared to the other species sampled here. These
408 general features are reflected in larger mean values for several size-invariant and local-
409 branching features and smaller mean values for many branch length dependent and size-
410 associated features, respectively (Fig. 5a).

411

412 **Multivariate, discriminant analysis of *Vitis* species based on inflorescence** 413 **architecture**

414

415 In order to understand how overall inflorescence architecture varies among *Vitis* species,
416 we performed PCA using all 24 morphological features and all samples. PC1 explained
417 37.12% of the total variation in the measured architecture (Fig. 6a). The traits with the
418 largest values for PC1 loadings, indicating that they contributed most to variation, are size-
419 associated features, Solidity and Sphericity. PC2 explained 15.4% of the total variation in
420 the measured inflorescence architecture, with variation primarily explained by local-
421 branching features such as PedicelDiameter, PedicelLength, PedicelLength/RachisLength,
422 AvgBranchLength, BranchDiameter, three berry potential traits, and PHn_PC1 (Fig. 6a).
423 Although inflorescences from each species occupy different regions of morphospace, these
424 regions overlap considerably.

425

426 LDA performed on the first 18 PCs, explaining 99.5% of the variation, distinguished
427 between species with a classification accuracy rate of 78.32%. A confusion matrix (Fig. 6b)
428 shows the proportion of samples correctly predicted for each species. LD1 primarily
429 separates *V. cinerea*, *V. labrusca*, and *V. amurensis* from the other species while LD2
430 primarily separates *V. vulpina* and *V. coignetiae*. The traits that are most important for
431 distinguishing these species, as indicated by LD loadings, are TotalBerryPotentialVolume
432 and PHn_PC1 for LD1, and AvgBranchLength and AvgBerryPotentialDiameter for LD2 (Fig.
433 6b). The most important predictors for correctly separating any two species are shown as
434 the grey scaled boxes in Fig. S6, and Table S3. For example, BranchDiameter and
435 PedicelDiameter are key when contrasting *V. coignetiae* and *V. vulpina*, suggesting that
436 different branch thickness easily distinguishes these two species. This method correctly
437 determined species classifications with 100% accuracy when contrasting *V. aestivalis* and
438 *V. cinerea*, *V. aestivalis* and *V. palmata*, *V. aestivalis* and *V. vulpina*, *V. amurensis* and *V. cinerea*,
439 *V. amurensis* and *V. palmata*, *V. cinerea* and *V. coignetiae*. Other combinations of species are
440 harder to distinguish on the basis of inflorescence characters. For example, the
441 classification accuracy rate was only 80% when distinguishing between *V. amurensis* and *V.*
442 *labrusca* and 82% for *V. aestivalis* and *V. coignetiae*.

443

444 **Phylogenetic signal of inflorescence architecture within clades**

445

446 The phylogeny dataset (N=99) is generally well-supported at the species level and
447 correlates well with current taxonomy. Using average trait values per individual, Pagel's
448 lambda shows 12 morphological traits (seven size-associated features along with
449 PedicelDiameter, TotalBerryPotentialVolume, Sphericity, PH_PC2, PHn_PC1) have strong
450 phylogenetic signal ($\lambda > 0.8$, Fig. 7, Table S4). While most species sampled tend to
451 have small values for the seven size-associated features, *V. aestivalis*, *V. cinerea*, and *V.*
452 *vulpina* tend to have values that are either close to median, or larger. On average, *V.*
453 *labrusca* has larger values for Sphericity and PHn_PC1 compared to other species sampled,
454 while *V. cinerea* generally has some of the smallest values for these traits. Only two
455 morphological traits (2nd/LongBranchLength, $\lambda = 0.06$ and
456 BerryPotentialTouchingDensity, $\lambda = 0.25$) lack phylogenetic signal (Fig.7, Table S4).

457
458 We observe differences in *Vitis* inflorescence architecture among clades and between
459 species. For North American (NA) clade I (*V. acerifolia*, *V. riparia*, *V. rupestris*), variation in
460 the 24 morphological traits measured have similarly small values among species,
461 particularly for several size-associated traits, although there is relatively large variation for
462 PH_PC3 and BerryPotentialTouchingDensity (Fig. 7). Within NA Clade I, we observe
463 differences among clade members for traits such as Sphericity and PHn_PC1 (larger in *V.*
464 *rupestris* compared to other clade members) and PedicelDiameter and BranchDiameter
465 (slightly larger in *V. acerifolia* compared to other clade members; Fig. 7). NA Clade II
466 appears to be more variable among clade members. *V. cinerea* has larger values for size-
467 associated traits compared to clade members *V. labrusca*, *V. palmata*, and *V. vulpina*.
468 Meanwhile, *V. labrusca* typically has larger values for local features (e.g., Sphericity,
469 PedicelDiameter, AvgBerryPotentialDiameter, PedicelBranchAngle) compared to the other
470 clade members (Fig. 7).

471
472 We calculated the mean value for each species of each morphological trait to study
473 variation within the three clades and detect subtle signatures (Fig. 7). We computed the
474 variance for the multivariate trait (combining all the 24 traits), and each of these 24 traits
475 for each clade (Fig. S4, Table S5). Overall, based on the samples used in this analysis,
476 variance of the multivariate trait for the NA Clade I (variation=0.14) is much smaller than
477 the NA Clade II (variation=0.64), while the variation for Asian Clade is 0.39. Some traits
478 have almost no variance in Asian Clade such as PedicelDiameter, PHn_PC2, PH_PC3, and
479 2nd/LongestBranchLength. However, North American species (8/~19 taxa) in this study
480 are better represented than Asian species (2/~37 taxa), so we are cautious not to
481 overinterpret this finding. Traits with the greatest variance in the Asian Clade included
482 PedicelLength/RachisLength, RachisLength, and PH_PC1, while NA Clade I has greatest
483 variance in PHn_PC2. All the other traits have greatest variance in the NA Clade II (Fig. S4,
484 Table S5). Traits with the smallest variance in the Asian Clade included PHn_PC3, PHn_PC1,
485 PedicelDiameter, BranchDiameter, NumberOfPedicel, 2nd/LongestBranchLength, PH_PC3,
486 and BerryPotentialTouchingDensity. The other traits had small variance in NA Clades I (Fig.
487 S4, Table S5). Our results highlight clade-specific variation in inflorescence architecture for
488 previously undescribed traits.

489 490 **Discussion**

491
492 Inflorescence architecture provides the scaffold on which flowers and fruits develop, and
493 consequently is a primary trait under investigation in many crop systems. Studies extend
494 into interspecific variation, pollen dispersal, genetic architecture, evolution, regulation, and
495 development of inflorescence structures (e.g., Bradley *et al.*, 1996; Friedman & Harder,
496 2004; Kellogg, 2007; Morris *et al.*, 2013; Han *et al.*, 2014; Hodge & Kellogg, 2015; Whipple,
497 2017; Stitzer & Ross-Ibarra, 2018; Ta *et al.*, 2018; Richter *et al.*, 2018). Yet the challenge
498 remains to analyze these complex 3D branching structures with appropriate tools. High
499 resolution data sets are required to represent the actual structure and comprehensive
500 analysis of both the geometric and topological features relevant to phenotypic variation
501 and to clarify evolutionary and developmental inflorescence patterns.

502

503 Our results demonstrate the power and potential of X-ray imaging and advanced
504 morphometric analysis for investigating complex 3D phenotypic features. We analyzed the
505 phenotypic variation in inflorescence architecture of 10 wild *Vitis* species using computer
506 vision and an emerging biological shape analysis method, persistent homology, which
507 allowed comprehensive comparisons of shape. Although samples analyzed here represent
508 only a subset of the known variation in *Vitis*, which includes an estimated 60 species, our
509 analyses demonstrate significant variation within and among *Vitis* species and among
510 clades. Correlation analysis (Fig. 5b) showed that PH is a complementary feature, as it is
511 relatively independent from most geometric features. We were able to assign widely
512 differing architectures to biological species with high accuracy (Fig. 6) from the 24
513 different morphometric traits surveyed in this study. PH provides an important
514 contribution to this discriminatory power, as does berry potential (Fig. 6b). We observed
515 that traits such as the rachis length, the sum of all branches, the space encompassing the
516 inflorescence architecture (ConvexHullVolume), and PH can be indicative of species and
517 clade (Fig. 7). Our results suggest meaningful, comprehensive information about the
518 inflorescence structure was captured with a single measure (i.e., the persistence barcode)
519 and that PH is a valuable method for quantifying and summarizing topological information.

520

521 Persistent homology analysis has led to a deeper understanding of trait genetic variation
522 and architecture in plants. Li *et al.* (2018a) used PH to analyze two-dimensional (2D) leaf
523 shape and predicted family identity with accuracy greater than expected by chance in over
524 140 plant families, outperforming other widely-used methods of digital shape analysis. Li *et al.*
525 (2018b) showed that PH-based, topological data analysis distinguished between
526 genotypes and identified many new quantitative trait loci (QTL) with 2D tomato leaf shape
527 and root architecture data. This work sets a precedent for measuring observable, yet
528 previously undescribed, phenotypes. In grapevine, QTL analysis indicates a genetic basis to
529 inflorescence architecture and berry compactness (Correa *et al.*, 2014; Richter *et al.*, 2018).
530 Deploying PH-based, topological modeling to grapevine mapping populations could lead to
531 the rapid identification of additional inflorescence trait QTL for breeding. For example, we
532 observed total branch length (a proxy for bigger or smaller clusters) correlates with
533 number of pedicels (a proxy for berry number; Fig. 5), an informative relationship to assess
534 potential yield. However, selecting for total branch length might lead to a negative
535 correlation with the average berry potential diameter (i.e., smaller berries). Although this
536 correlation may be desirable for wine grapes, it is not for table grapes.

537

538 Grapevine cluster architecture is a composite feature that reflects multiple subtraits
539 including stalk traits (inflorescence architecture) and berry features (Richter *et al.*, 2018).
540 OIV 204 uses “bunch: density” to describe variation in clusters, ranging from (1) berries
541 clearly separated with many visible pedicels to (9) berries deformed by compression (OIV,
542 2001; Rombough, 2002). Other authors have deconstructed traits contributing to cluster
543 architecture primarily through individual measurements taken by hand (e.g., Shavrukov *et al.*,
544 2004; Tello *et al.*, 2015; Zdunić *et al.*, 2015; Tello & Ibáñez, 2018) and more recently,
545 with image-based technologies (Cubero *et al.*, 2014; Roscher *et al.*, 2014; Ivorra *et al.*, 2015;
546 Aquino *et al.*, 2017, 2018; Rist *et al.*, 2018). Here, we are able to describe traits of interest
547 that contribute greatly to the morphological features captured by the OIV scale (e.g.,

548 NumberOfPedicel, PedicelLength, PedicelBranchAngle, RachisLength, overall shape using
549 PH; Fig 2, Fig. S2). This method could facilitate precision breeding for both whole
550 inflorescence structure topology and specific desirable geometric traits.

551
552 While several studies have quantified cluster structure in cultivated grapevines, similar
553 studies of wild *Vitis* inflorescence architecture are lacking. Munson (1909) and Galet
554 (1979) describe North American *Vitis* cluster structure qualitatively, commenting on
555 compactness, size, shape, and the presence of large first primary branches
556 (wings/shoulders). Taxonomic descriptions typically do not examine inflorescence
557 architecture beyond categorical type, position on the vine, and the average number of
558 berries per cluster (Comeaux *et al.*, 1987; Moore, 1991; Moore & Wen, 2016). Descriptions
559 of the position of the inflorescence are useful for identification and are included in
560 dichotomous keys; however, to our knowledge, other inflorescence architecture traits have
561 not been rigorously quantified among wild *Vitis* species. Although qualitative descriptions
562 are valuable and accessible, powerful phenotyping tools are required to associate complex
563 phenotypes with evolutionary and developmental patterns.

564
565 Using 3D imaging and PH with a topological modeling approach, we identified attributes of
566 inflorescence architecture that vary within and among *Vitis* species that, to our knowledge,
567 have not been previously described. Differences in inflorescence architecture among clades
568 mirror other phenotypic differences among members of North American *Vitis*. For example,
569 members of NA Clade I (*V. acerifolia*, *V. riparia*, and *V. rupestris*) have small values for size-
570 associated features (e.g., RachisLength, ConvexHullVolume, NumberOfPedicel,
571 TotalBranchLength, SurfaceArea, Volume) and relatively large values for PH_PC3 and
572 BerryPotentialTouchingDensity (Fig. 7). These species share suites of other morphological
573 characters (nodal diaphragm, branch, and leaf surface traits, and large stipules; Moore
574 1991, Moore and Wen 2016, Klein *et al.*, 2018). It is possible that among closely related
575 species conserved pathways generate vegetative and reproductive similarities.

576
577 Sample size is low for the Asian Clade and most of NA Clade II, limiting our ability to assess
578 variation in these species; however, members of NA Clade II do not have suites of shared
579 inflorescence traits (*V. aestivalis*, *V. cinerea*, *V. labrusca*, *V. vulpina*; Klein *et al.*, 2018).
580 Rather, *V. labrusca* has very small values for size-associated traits and larger values for
581 local features compared to the other clade members, whereas *V. cinerea* has larger values
582 for size-associated features and smaller values for local features (Fig. 7). This is consistent
583 with the observation that aside from core phenotypic synapomorphies in the genus
584 (tendrils, bark, lenticel, and nodal diaphragm characters), members of NA Clade IIb (*V.*
585 *aestivalis*, *V. cinerea*, *V. labrusca*, and *V. vulpina*) do not share morphological traits unique to
586 the clade (Klein *et al.*, 2018). These species mostly co-occur across their distributions
587 (Callen *et al.*, 2016) and additional sampling of *Vitis* taxa is necessary to further explore
588 these complex evolutionary patterns. We observe *V. amurensis* grouping with *V. labrusca*
589 and *V. coignetiae* grouping with North American species in hierarchical cluster analysis
590 (Fig. 5a). The former two species have relatively smaller inflorescence architectures with
591 thicker branches compared to the other species sampled here. Taxonomic relationships
592 among North American and Asian *Vitis* species have been historically challenging, with
593 clades comprised of species with disjunct distributions (Mullins *et al.*, 1992). Since current

594 taxonomy resolves separate Asian and North American clades (Klein *et al.*, 2018),
595 morphological similarity between these species likely reflects convergent evolution.

596

597

598 **Future Directions**

599

600 Three-dimensional imaging through XRT and advanced mathematical approaches like
601 persistent homology provide new ways to visualize and interpret complex biological
602 structures including inflorescences, and to understand the genetic and environmental
603 factors underlying variation in their architecture. In grapevines, cluster density is an
604 important trait that is used to assess grapevine crop quality and to forecast yield, in part
605 because of the association between bunch density and fungal infestations such as *Botrytis*
606 (Hed *et al.*, 2009; Iland *et al.*, 2011; Molitor & Beyer, 2014; Molitor *et al.*, 2018). This study
607 expands on previous work identifying variation in inflorescence architecture among
608 cultivars (Shavrukov *et al.*, 2004), finding notable differences in cluster architecture among
609 species. A logical next step may be to use 3D images and PH with topological modeling to
610 trace the development of inflorescences across multiple growing seasons in a mapping
611 population. Methods presented here are also amenable to scanning with berries, provided
612 some noteworthy technical challenges are first addressed (e.g. minimizing berry damage
613 and rotting during transportation, cluster stabilization during scanning, and segmentation
614 of 3D volumes with features that vary widely in their X-ray absorbance). This work would
615 provide a more complete representation of cluster structure, as well as inform our berry
616 potential simulation with genotype-specific empirical data. We plan to develop predictive
617 structural models of grapevine cluster development using these techniques.

618

619 Imaging and shape analysis approaches presented here can also be used to tease apart
620 subtle environmental influences on inflorescence architecture, and the major agronomic
621 trait of bunch density. Identifying environmental effects on phenotypic variation has
622 important implications both for vineyard management and the assessment of intra-clone
623 variation across geographic space. Cluster compactness can be manipulated through a
624 variety of agronomic practices ([Molitor et al. 2012](#); [Gil et al. 2013](#); [Frioni et al. 2017](#);
625 [Gourieroux et al. 2017](#); [Poni et al. 2018](#); [Reeve et al. 2018](#)). Techniques described here can
626 be used to quantify influences of specific treatments on cluster architecture. In addition,
627 because grapevines are clonally propagated, clusters from the same widespread clones can
628 be collected from different geographic locations, scanned and analyzed for variation. High
629 resolution assessment of inflorescence architecture offers important insights into natural
630 variation in bunch density and the genetic and environmental factors that influence it. The
631 capacity to capture 3D variation in this complex trait over space and time represents a
632 promising advance for a valuable potential target of selection in one of the most
633 economically important berry crops in the world.

634

635

636 **Acknowledgements**

637

638 The authors would like to acknowledge Elizabeth A. Kellogg (DDPSC) for valuable
 639 comments, particularly on phylogenetic analysis and inflorescence anatomy. We thank
 640 Noah Fahlgren (DDPSC) for computational assistance and Kari Miller (Washington
 641 University) for scanning assistance. We thank Zoë Migicovsky (Dalhousie University) for
 642 valuable comments.

643

644 **Author contributions**

645

646 CNT and JL designed the research; JL collected the samples and consulted on the biology;
 647 KD generated the X-ray data; LLK and AJM provided phylogenetic data and consulted for
 648 the biology; NJ and ML extracted pedicel diameter and angle; ML developed and extracted
 649 all the traits and conducted all the analysis and figures; ML, LLK, KD, JL, AJM, and CNT
 650 wrote the manuscript.

651

652 **Tables**

653

654

Table 1 Number of samples/individuals each species and berry information used in the study

	Number (N)			Berry information (Galet (1988); Moore and Wen (2016))		
	Sam ples	Individ uals	Individuals used in phylogenetic analysis	low diameter (mm)	High diameter (mm)	Berries per bunch
<i>V. acerifoli a</i>	32	11	9	8	12	>25
<i>V. aestival is</i>	5	2	1	8	20	>25
<i>V. amuren sis</i>	13	5	2	8	15	NA
<i>V. cinerea</i>	45	15	13	4	8	>25
<i>V. coigneti ae</i>	6	2	1	NA	8	NA
<i>V. labrusc a</i>	62	22	12	12	23	<25
<i>V. palmat a</i>	3	1	1	8	10	>25

<i>V. riparia</i>	158	53	48	8	12	>25
<i>V. rupestris</i>	41	16	10	8	12	<25
<i>V. vulpina</i>	27	9	2	8	12	>25
Total	392	136	99			

655
656

Table 2. Fifteen geometric traits were organized into three categories based on the type of shape information captured by the trait. See STable 1. for a more detailed description of each trait.

Global-size features	Local-branching features	Size-invariant features
Volume*	RachisLength*	Solidity
ConvexHullVolume*	PedicelLength	Sphericity
SurfaceArea*	AvgBranchLength	2nd/LongestBranchLength
TotalBranchLength*	BranchDiameter	PedicelLength/RachisLength
NumberOfPedicel*	PedicelDiameter	
	PedicelBranchAngle	
Size-associated features (traits with * +PH_PC1)		

657
658
659
660

Supporting Information

661 **Fig. S1** A maximum likelihood phylogenetic tree for ten *Vitis* species.
662 **Fig. S2** Summary of inflorescence geometric and topological traits and the distribution for
663 ten *Vitis* species.
664 **Fig. S3** Morphological traits mapped on the phylogenetic tree.
665 **Fig. S4.** Variation for each clade.
666 **Fig. S5** Pairwise correlations of morphological traits (allometric relationships) showing
667 linear regression lines for each species.
668 **Fig. S6** Pairwise species classification.
669 **Table S1.** Trait description and calculation.
670 **Table S2.** Trait variance for each species.
671 **Table S3.** Trait loadings for two species classification.
672 **Table S4.** Trait Pagel's lambda for phylogenetic analysis.
673 **Table S5.** Trait variation for each clade.
674 **Video S1** Illustration of quantifying branching topology using persistent homology.
675 **Video S2** Berry potential simulation

676
677

678 **References**

679

680 **Aquino A, Diago MP, Millán B, Tardáguila J. 2017.** A new methodology for estimating the
681 grapevine-berry number per cluster using image analysis. *Biosystems Engineering* **156**: 80–
682 95.

683 **Aquino A, Barrio I, Diago M-P, Millan B, Tardaguila J. 2018.** vitisBerry: An Android-
684 smartphone application to early evaluate the number of grapevine berries by means of
685 image analysis. *Computers and Electronics in Agriculture* **148**: 19–28.

686 **Bettiga LJ. 2003.** *Wine grape varieties in California*. UCANR Publications.

687 **Bioletti F. 1938.** Outline of ampelography for the vinifera grapes in California. *Hilgardia*
688 **11**: 227–293.

689 **Bradley D, Carpenter R, Copsey L, Vincent C, Rothstein S, Coen E. 1996.** Control of
690 inflorescence architecture in *Antirrhinum*. *Nature* **379**: 791–797.

691 **Brereton NJB, Ahmed F, Sykes D, Ray MJ, Shield I, Karp A, Murphy RJ. 2015.** X-ray
692 micro-computed tomography in willow reveals tissue patterning of reaction wood and
693 delay in programmed cell death. *BMC plant biology* **15**: 83.

694 **Bucksch A, Atta-Boateng A, Azihou AF, Battogtokh D, Baumgartner A, Binder BM,**
695 **Braybrook SA, Chang C, Coneva V, DeWitt TJ, et al. 2017.** Morphological Plant Modeling:
696 Unleashing Geometric and Topological Potential within the Plant Sciences. *Frontiers in*
697 *plant science* **8**: 900.

698 **Callen ST, Klein LL, Miller AJ. 2016.** Climatic Niche Characterization of 13 North
699 American *Vitis* Species. *American journal of enology and viticulture* **67**: 339-349

700 **Chanderbali AS, Berger BA, Howarth DG, Soltis PS, Soltis DE. 2016.** Evolving ideas on
701 the origin and evolution of flowers: new perspectives in the genomic era. *Genetics* **202**:
702 1255–1265.

703 **Chifman J, Kubatko L. 2014.** Quartet inference from SNP data under the coalescent model.
704 *Bioinformatics* **30**: 3317–3324.

705 **Cignoni P, Callieri M, Corsini M, Dellepiane M, Ganovelli F, Ranzuglia G. 2008.**
706 Meshlab: an open-source mesh processing tool. In: *Eurographics Italian chapter conference*.
707 129–136.

708 **Cohen-Steiner D, Edelsbrunner H, Harer J. 2007.** Stability of Persistence Diagrams.
709 *Discrete & computational geometry* **37**: 103–120.

710 **Comeaux BL, Nesbitt WB, Fantz PR. 1987.** Taxonomy of the Native Grapes of North
711 Carolina. *Castanea* **52**: 197–215.

- 712 **Coombe BG. 1995.** Adoption of a system for identifying grapevine growth stages. *Growth*
713 *stages of the grapevine Australian Journal of Grape and Wine Research* **1**: 100–110.
- 714 **Correa J, Mamani M, Muñoz-Espinoza C, Laborie D, Muñoz C, Pinto M, Hinrichsen P.**
715 **2014.** Heritability and identification of QTLs and underlying candidate genes associated
716 with the architecture of the grapevine cluster (*Vitis vinifera* L.). *Theoretical and applied*
717 *genetics.* **127**: 1143–1162.
- 718 **Cubero S, Diago MP, Blasco J, Tardáguila J, Millán B, Aleixos N. 2014.** A new method for
719 pedicel/peduncle detection and size assessment of grapevine berries and other fruits by
720 image analysis. *Biosystems Engineering* **117**: 62–72.
- 721 **Delory BM, Li M, Topp CN, Lobet G. 2018.** archiDART v3.0: A new data analysis pipeline
722 allowing the topological analysis of plant root systems. *F1000Research* **7**: 22.
- 723 **Doebley J, Stec A, Hubbard L. 1997.** The evolution of apical dominance in maize. *Nature*
724 **386**: 485–488.
- 725 **Earles JM, Knipfer T, Tixier A, Orozco J, Reyes C, Zwieniecki MA, Brodersen CR,**
726 **McElrone AJ. 2018.** In vivo quantification of plant starch reserves at micrometer
727 resolution using X-ray microCT imaging and machine learning. *The New phytologist* **218**:
728 1260-1269.
- 729 **Edelsbrunner H, Morozov D. 2013.** Persistent homology: theory and practice.In:
730 *Proceedings of the European congress of mathematics*, 31-50.
- 731 **Elshire RJ, Glaubitz JC, Sun Q, Poland JA, Kawamoto K, Buckler ES, Mitchell SE. 2011.** A
732 robust, simple genotyping-by-sequencing (GBS) approach for high diversity species. *PLoS*
733 *one* **6**: e19379.
- 734 **Endress PK. 2010.** Disentangling confusions in inflorescence morphology: patterns and
735 diversity of reproductive shoot ramification in angiosperms. *Journal of systematics and*
736 *evolution* **48**: 225–239.
- 737 **Feng C-M, Xiang Q-YJ, Franks RG. 2011.** Phylogeny-based developmental analyses
738 illuminate evolution of inflorescence architectures in dogwoods (*Cornus* s. l., Cornaceae).
739 *The New phytologist* **191**: 850–869.
- 740 **Friedman J, Harder LD. 2004.** Inflorescence architecture and wind pollination in six grass
741 species. *Functional ecology* **18**: 851–860.
- 742 **Frioni T, Zhuang S, Palliotti A, Sivilotti P, Falchi R, Sabbatini P. 2017.** Leaf Removal and
743 Cluster Thinning Efficiencies Are Highly Modulated by Environmental Conditions in Cool
744 Climate Viticulture. *American journal of enology and viticulture: ajev*.2017.16098.
- 745 **Galet P. 1979.** *A practical ampelography*. Cornell University Press.
- 746 **Galet P. 1988.** *Cépages et Vignobles de France. Tome I: Les Vignes Américaines*. Imprimerie

- 747 Déhan, Montpellier.
- 748 **Gil M, Esteruelas M, González E, Kontoudakis N, Jiménez J, Fort F, Canals JM,**
749 **Hermosín-Gutiérrez I, Zamora F. 2013.** Effect of two different treatments for reducing
750 grape yield in *Vitis vinifera* cv Syrah on wine composition and quality: berry thinning
751 versus cluster thinning. *Journal of agricultural and food chemistry* **61**: 4968–4978.
- 752 **Godin C, Caraglio Y. 1998.** A Multiscale Model of Plant Topological Structures. *Journal of*
753 *theoretical biology* **191**: 1–46.
- 754 **Godin C, Costes E, Sinoquet H. 1999.** A Method for Describing Plant Architecture which
755 Integrates Topology and Geometry. *Annals of botany* **84**: 343–357.
- 756 **Gomez FE, Carvalho G Jr, Shi F, Muliana AH, Rooney WL. 2018.** High throughput
757 phenotyping of morpho-anatomical stem properties using X-ray computed tomography in
758 sorghum. *Plant methods* **14**: 59.
- 759 **Gourieroux AM, Holzapfel BP, McCully ME, Scollary GR, Rogiers SY. 2017.** Vascular
760 development of the grapevine (*Vitis vinifera* L.) inflorescence rachis in response to flower
761 number, plant growth regulators and defoliation. *Journal of plant research* **130**: 873–883.
- 762 **Guédon Y, Barthélémy D, Caraglio Y, Costes E. 2001.** Pattern Analysis in Branching and
763 Axillary Flowering Sequences. *Journal of theoretical biology* **212**: 481–520.
- 764 **Hake S. 2008.** Inflorescence Architecture: The Transition from Branches to Flowers.
765 *Current biology: CB* **18**: R1106–R1108.
- 766 **Han Y, Yang H, Jiao Y. 2014.** Regulation of inflorescence architecture by cytokinins.
767 *Frontiers in plant science* **5**: 669.
- 768 **Haus MJ, Li M, Chitwood DH, Jacobs TW. 2018.** Long-Distance and Trans-Generational
769 Stomatal Patterning by CO₂ Across Arabidopsis Organs. *Frontiers in plant science* **9**: 1714.
- 770 **Hed B, Ngugi HK, Travis JW. 2009.** Relationship Between Cluster Compactness and Bunch
771 Rot in Vignoles Grapes. *Plant disease* **93**: 1195–1201.
- 772 **Hertweck KL, Pires JC. 2014.** Systematics and Evolution of Inflorescence Structure in the
773 *Tradescantia* Alliance (Commelinaceae). *Systematic botany* **39**: 105–116.
- 774 **Hodel DR Greby K, Ohara LM, Ohara ET. 2015.** Infructescence and fruit characteristics of
775 Washingtonia (Arecaceae: Coryphoideae). *PalmArbor* **2**: 1–7.
- 776 **Hodge JG, Kellogg EA. 2015.** Patterns of Inflorescence Development of Three Prairie
777 Grasses (Andropogoneae, Poaceae). *International journal of plant sciences* **175**(9): 963–974.
- 778 **Hughes N, Askew K, Scotson CP, Williams K, Sauze C, Corke F, Doonan JH, Nibau C.**
779 **2017.** Non-destructive, high-content analysis of wheat grain traits using X-ray micro
780 computed tomography. *Plant methods* **13**: 76.

- 781 **Iland P, Dry P, Proffitt T, Tyerman S. 2011.** *The grapevine: from the science to the practice*
782 *of growing vines for wine*. Patrick Iland Wine Promotions Adelaide.
- 783 **Ivorra E, Sánchez AJ, Camarasa JG, Diago MP, Tardaguila J. 2015.** Assessment of grape
784 cluster yield components based on 3D descriptors using stereo vision. *Food control* **50**:
785 273–282.
- 786 **Jhala VM, Thaker VS. 2015.** X-ray computed tomography to study rice (*Oryza sativa* L.)
787 panicle development. *Journal of experimental botany* **66**: 6819–6825.
- 788 **Kang M-Z, Cournède P-H, Mathieu A, Letort V, Qi R, Zhan Z-G. 2009.** A Functional-
789 Structural Plant Model—Theories and Its Applications in Agronomy. In: *Crop Modeling and*
790 *Decision Support*. Springer Berlin Heidelberg, 148–160.
- 791 **Kellogg EA. 2007.** Floral displays: genetic control of grass inflorescences. *Current opinion*
792 *in plant biology* **10**: 26–31.
- 793 **Kirchoff BK, Claßen-Bockhoff R. 2013.** Inflorescences: concepts, function, development
794 and evolution. *Annals of botany* **112**: 1471–1476.
- 795 **Klein LL, Miller AJ, Ciotir C, Hyma K, Uribe-Convers S, Londo J. 2018.** High-throughput
796 sequencing data clarify evolutionary relationships among North American *Vitis* species and
797 improve identification in USDA *Vitis* germplasm collections. *American journal of botany*
798 **105**: 215–226.
- 799 **Kuijt J. 1981.** Inflorescence morphology of Loranthaceae. *Blumea* **27**: 1-73.
- 800 **Kumar S, Stecher G, Li M, Knyaz C, Tamura K. 2018.** MEGA X: Molecular Evolutionary
801 Genetics Analysis across Computing Platforms. *Molecular biology and evolution* **35**: 1547–
802 1549.
- 803 **Landrein S, Prenner G, Chase MW, Clarkson JJ. 2012.** Abelia and relatives: phylogenetics
804 of Linnaeae (Dipsacales–Caprifoliaceae s.l.) and a new interpretation of their inflorescence
805 morphology. *Botanical journal of the Linnean Society* **169**: 692–713.
- 806 **Le C-T, Liu B, Barrett RL, Lu L-M, Wen J, Chen Z-D. 2018.** Phylogeny and a new tribal
807 classification of Opiliaceae (Santalales) based on molecular and morphological evidence:
808 Phylogeny and classification of Opiliaceae. *Journal of Systematics and Evolution* **56**: 56–66.
- 809 **Letort V, Cournede P, Lecoeur J, Hummel I, Reffye PD, Christophe A. 2006.** Effect of
810 Topological and Phenological Changes on Biomass Partitioning in *Arabidopsis thaliana*
811 Inflorescence: A Preliminary Model-Based Study. In: *Plant Growth Modeling, Simulation,*
812 *Visualization and Application*, eds Thierry F and Zhang XP, IEEE Computer Society: 65–69.
- 813 **Li M, Duncan K, Topp CN, Chitwood DH. 2017.** Persistent homology and the branching
814 topologies of plants. *American journal of botany* **104**: 349–353.
- 815 **Li M, An H, Angelovici R, Bagaza C, Batushansky A, Clark L, Coneva V, Donoghue MJ,**

- 816 **Edwards E, Fajardo D, et al. 2018a.** Topological Data Analysis as a Morphometric Method:
817 Using Persistent Homology to Demarcate a Leaf Morphospace. *Frontiers in plant science* **9**:
818 553.
- 819 **Li M, Frank MH, Coneva V, Mio W, Chitwood DH, Topp CN. 2018b.** The Persistent
820 Homology Mathematical Framework Provides Enhanced Genotype-to-Phenotype
821 Associations for Plant Morphology. *Plant physiology* **177**: 1382–1395.
- 822 **Marguerit E, Boury C, Manicki A, Donnart M, Butterlin G, Némorin A, Wiedemann-**
823 **Merdinoglu S, Merdinoglu D, Ollat N, Decroocq S. 2009.** Genetic dissection of sex
824 determinism, inflorescence morphology and downy mildew resistance in grapevine. *TAG.*
825 *Theoretical and applied genetics. Theoretische und angewandte Genetik* **118**: 1261–1278.
- 826 **Mathers AW, Hepworth C, Baillie AL, Sloan J, Jones H, Lundgren M, Fleming AJ,**
827 **Mooney SJ, Sturrock CJ. 2018.** Investigating the microstructure of plant leaves in 3D with
828 lab-based X-ray computed tomography. *Plant methods* **14**: 99.
- 829 **McAllister CA, McKain MR, Li M, Bookout B, Kellogg EA 2019.** Specimen-based analysis
830 of morphology and the environment in ecologically dominant grasses: the power of the
831 herbarium. *Philosophical transactions of the Royal Society B: Biological sciences* **374**:
832 20170403.
- 833 **Migicovsky Z, Li M, Chitwood DH, Myles S. 2018.** Morphometrics reveals complex and
834 heritable apple leaf shapes. *Front. Plant Sci.* **8**: 2185.
- 835 **Miller AJ, Matasci N, Schwaninger H, Aradhya MK, Prins B, Zhong G-Y, Simon C,**
836 **Buckler ES, Myles S. 2013.** *Vitis* phylogenomics: hybridization intensities from a SNP array
837 outperform genotype calls. *PLoS one* **8**: e78680.
- 838 **Molitor D, Behr M, Hoffmann L, Evers D. 2012.** Impact of Grape Cluster Division on
839 Cluster Morphology and Bunch Rot Epidemic. *American journal of enology and viticulture*
840 **63**: 508–514.
- 841 **Molitor D, Beyer M. 2014.** Epidemiology, identification and disease management of grape
842 black rot and potentially useful metabolites of black rot pathogens for industrial
843 applications - a review. *The Annals of applied biology* **165**: 305–317.
- 844 **Molitor D, Biewers B, Junglen M, Schultz M, Clementi P, Permesang G, Regnery D,**
845 **Porten M, Herzog K, Hoffmann L, et al. 2018.** Multi-annual comparisons demonstrate
846 differences in the bunch rot susceptibility of nine *Vitis vinifera* L. 'Riesling' clones. *Vitis* **57**:
847 17-25.
- 848 **Moore MO. 1991.** Classification and systematics of eastern North American *Vitis* L.
849 (vitaceae) north of Mexico. *SIDA, contributions to botany* **14**: 339–367.
- 850 **Moore M, Wen J. 2016.** Vitaceae. In: *Flora of North America North of Mexico*, ed. Flora of
851 North America Editorial Committee. 3–23.

- 852 **Morris GP, Ramu P, Deshpande SP, Hash CT, Shah T, Upadhyaya HD, Riera-Lizarazu O,**
853 **Brown PJ, Acharya CB, Mitchell SE, et al. 2013.** Population genomic and genome-wide
854 association studies of agroclimatic traits in sorghum. *Proceedings of the National Academy*
855 *of Sciences of the United States of America* **110**: 453–458.
- 856 **Mullins MG, Bouquet A, Williams LE. 1992.** *Biology of the grapevine*. Cambridge
857 University Press.
- 858 **Munson TV. 1909.** *Foundations of American Grape Culture*. Orange Judd Company.
- 859 **OIV. 2001.** *2nd Edition of the Oiv Descriptor List for Grape Varieties and Vitis species*.
- 860 **Périlleux C, Lobet G, Tocquin P. 2014.** Inflorescence development in tomato: gene
861 functions within a zigzag model. *Frontiers in plant science* **5**: 121.
- 862 **Pfeifer J, Kirchgessner N, Colombi T, Walter A. 2015.** Rapid phenotyping of crop root
863 systems in undisturbed field soils using X-ray computed tomography. *Plant methods* **11**: 41.
- 864 **Poni S, Gatti M, Palliotti A, Dai Z, Duchêne E, Truong T-T, Ferrara G, Matarrese AMS,**
865 **Gallotta A, Bellincontro A, et al. 2018.** Grapevine quality: A multiple choice issue. *Scientia*
866 *horticulturae* **234**: 445–462.
- 867 **Prusinkiewicz P, Erasmus Y, Lane B, Harder LD, Coen E. 2007.** Evolution and
868 development of inflorescence architectures. *Science* **316**: 1452–1456.
- 869 **Pulliat V. 1888.** *Mille variétés de vignes, description et synonymies*, Paris Montpellier.
- 870 **Reeve AL, Skinkis PA, Vance AJ, McLaughlin KR, Tomasino E, Lee J, Tarara JM. 2018.**
871 Vineyard Floor Management and Cluster Thinning Inconsistently Affect ‘Pinot noir’ Crop
872 Load, Berry Composition, and Wine Quality. *HortScience: a publication of the American*
873 *Society for Horticultural Science* **53**: 318–328.
- 874 **Revell LJ. 2012.** phytools: an R package for phylogenetic comparative biology (and other
875 things). *Methods in ecology and evolution* **3**: 217–223.
- 876 **de Ribou S de B, Douam F, Hamant O, Frohlich MW, Negrutiu I. 2013.** Plant science and
877 agricultural productivity: Why are we hitting the yield ceiling? *Plant science: an*
878 *international journal of experimental plant biology* **210**: 159–176.
- 879 **Richter R, Gabriel D, Rist F, Töpfer R, Zyprian E. 2018.** Identification of co-located QTLs
880 and genomic regions affecting grapevine cluster architecture. *Theoretical and applied*
881 *genetics*. doi.org/10.1007/s00122-018-3269-1
- 882 **Rist F, Herzog K, Mack J, Richter R, Steinhage V, Töpfer R. 2018.** High-Precision
883 Phenotyping of Grape Bunch Architecture Using Fast 3D Sensor and Automation. *Sensors*
884 **18**: 763.
- 885 **Rombough L. 2002.** *The Grape Grower: A Guide to Organic Viticulture*. Chelsea Green
886 Publishing.

- 887 **Roscher R, Herzog K, Kunkel A, Kicherer A, Töpfer R, Förstner W. 2014.** Automated
888 image analysis framework for high-throughput determination of grapevine berry sizes
889 using conditional random fields. *Computers and Electronics in Agriculture* **100**: 148–158.
- 890 **Rovasenda J. 1881.** Essai d'une ampélographie universelle. traduit de l'Italien par
891 F.Cazalis, G. Foëx et al., Paris Montpellier.
- 892 **Shavrukov YN, Dry IB, Thomas MR. 2004.** Inflorescence and bunch architecture
893 development in *Vitis vinifera* L. *Australian journal of grape and wine research* **10**: 116–124.
- 894 **Stitzer MC, Ross-Ibarra J. 2018.** Maize domestication and gene interaction. *New*
895 *phytologist* **220**: 395–408.
- 896 **Swofford DL. 2003.** PAUP*: phylogenetic analysis using parsimony, version 4.0 b10.
- 897 **Ta KN, Khong NG, Ha TL, Nguyen DT, Mai DC, Hoang TG, Phung TPN, Bourrie I,**
898 **Courtois B, Tran TTH, et al. 2018.** A genome-wide association study using a Vietnamese
899 landrace panel of rice (*Oryza sativa*) reveals new QTLs controlling panicle morphological
900 traits. *BMC plant biology* **18**: 282.
- 901 **Tello J, Aguirrezábal R, Hernáiz S, Larreina B, Montemayor MI, Vaquero E, Ibáñez J.**
902 **2015.** Multicultivar and multivariate study of the natural variation for grapevine bunch
903 compactness: Multicultivar study of grapevine bunch compactness. *Australian journal of*
904 *grape and wine research* **21**: 277–289.
- 905 **Tello J, Ibáñez J. 2018.** What do we know about grapevine bunch compactness? A state-of-
906 the-art review: Review on bunch compactness. *Australian journal of grape and wine*
907 *research* **24**: 6–23.
- 908 **Tröndle D, Schroder S, Kassemeyer H-H, Kiefer C, Koch MA, Nick P. 2010.** Molecular
909 phylogeny of the genus *Vitis* (Vitaceae) based on plastid markers. *American journal of*
910 *botany* **97**: 1168–1178.
- 911 **Venables WN, Ripley BD. 2002.** *Modern Applied Statistics with S. Fourth Edition.* Springer.
- 912 **Weberling F. 1992.** *Morphology of Flowers and Inflorescences.* Cambridge University Press.
- 913 **Wei T, Simko V. 2017.** R package 'corrplot': visualization of a correlation matrix (version
914 0.84). URL <https://github.com/taiyun/corrplot>.
- 915 **Whipple CJ. 2017.** Grass inflorescence architecture and evolution: the origin of novel
916 signaling centers. *New phytologist* **216**: 367–372.
- 917 **Wyatt R. 1982.** Inflorescence architecture: how flower number, arrangement, and
918 phenology affect pollination and fruit-set. *American journal of botany* **69**: 585–594.
- 919 **Zdunić G, Mucalo A, Budić-Leto I, Humar I, Pejić I, Maletić E.** Cluster architecture of old,
920 neglected Croatian grapevine varieties (*Vitis vinifera* L.). *Vitis* **54**: 177-180.

921 **Zecca G, Abbott JR, Sun W-B, Spada A, Sala F, Grassi F. 2012.** The timing and the mode of
922 evolution of wild grapes (*Vitis*). *Molecular phylogenetics and evolution* **62**: 736–747.

923 **Zhang N, Wen J, Zimmer EA. 2015.** Expression patterns of *AP1*, *FUL*, *FT* and *LEAFY*
924 orthologs in Vitaceae support the homology of tendrils and inflorescences throughout the
925 grape family: Evolution of tendrils in Vitaceae. *Journal of Systematics and Evolution* **53**:
926 469–476.

927
928

929 **Figure Legends**

930

931 **Fig. 1** Sample preparation and imaging. (a) The ten *Vitis* species sampled for this study
932 display diverse grape bunch morphology. (b) Inflorescence architectures after berry
933 removal. (c) Inside the X-ray tomography instrument; the inflorescence is clamped in a
934 panavise between two pieces of polystyrene on the X-ray turntable. (d) Two dimensional
935 radiogram of grape inflorescence; X-rays, absorbed or passing through the inflorescence,
936 are detected to create a silhouette. (e) Three dimensional reconstruction and the structure
937 of the same inflorescence shown in (d) by taking radiograms at successive different angles
938 and then computationally combining the images.

939

940 **Fig. 2** Examples of inflorescence geometric and topological traits and their distribution for
941 ten *Vitis* species. Each panel shows one of the three traits categories (geometric traits,
942 topological traits, and berry potential traits). Geometric traits are organized as global size
943 features, local branching features, and size-invariant features. Each trait is listed at the top
944 of the column and two inflorescence examples demonstrating low and high trait values
945 listed to the left. At the bottom of each column is a boxplot indicating the distribution and
946 variance within the ten *Vitis* species, represented in different colors. On each box, each dot
947 indicates an outlier if it is more than 1.5 interquartile ranges; the central vertical line
948 indicates the median; the left and right edges of the box represent the 25th and 75th
949 percentiles; and the whiskers extend to the most extreme nonoutlier data. The label for
950 each species is listed in the boxplot y axis of the leftmost plot, with the number of
951 individuals sampled for each species shown in parentheses. For a more complete example
952 and detailed description of each trait, see Fig. S2 and Table S1.

953

954 **Fig. 3** Persistent homology with geodesic distance comprehensively quantifies branching
955 structures. (a) A level (pink solid line) defined by the same geodesic distance (length of any
956 of the purple curves, in this case, set to 90) to the base of the inflorescence. The super level
957 set is the pixels (in black) having greater geodesic distance than the pink level. (b) Pixels on
958 a branching structure are colored by their geodesic distance to the base. They are colored
959 with red
960 representing the most distant through to blue for the closest ones. (c) A persistence
961 barcode for each branching structure records the connected components for each level set
962 at each geodesic distance value. The “birth” and “death” values for each bar represent the
963 level where each branch starts and gets merged. Colored bars correspond to colored
964 branches. (d) Above: example inflorescence. The stem is digitally cut at the base (brown

965 line) where it meets the first branch. Below: 3D surface on the example inflorescence as in
966 (b). (e) Persistence barcode for the inflorescence in (d). (f) and (g), similar to (d) and (e),
967 show a different inflorescence architecture.

968

969 **Fig. 4** Berry potential simulation to explore the space determined by inflorescence
970 architecture. (a) Determine the growth direction for each berry potential. (b) Expand berry
971 potential by increasing the size and moving the center along the growth direction until it
972 meets any of these three cases: 1) two berry potentials touch each other; 2) a berry
973 potential touches any part of the inflorescence; 3) the diameter of the berry potential
974 reaches the maximum for the species..

975

976

977 **Fig. 5** Hierarchical cluster analysis and correlation analysis. (a) Cluster analysis based the
978 mean value for each trait of 10 *Vitis* species. The heatmap shows values above (red) or
979 below (blue) the mean for each trait. The morphological traits (rows) are clustered
980 hierarchically with the name shown on the right and hierarchical tree listed on the left. The
981 species (columns) are also clustered hierarchically with the name and hierarchical tree
982 shown at the top. (b) Correlation matrix plot shows pairwise positively stronger
983 correlation (green and larger circle) or negatively stronger correlation (purple and larger
984 circle). Non-significant correlations ($p > 0.05$) are crossed out. The traits are ordered in the
985 same way as (a). (c) Selected pairs of traits showing linear regression lines for each species.

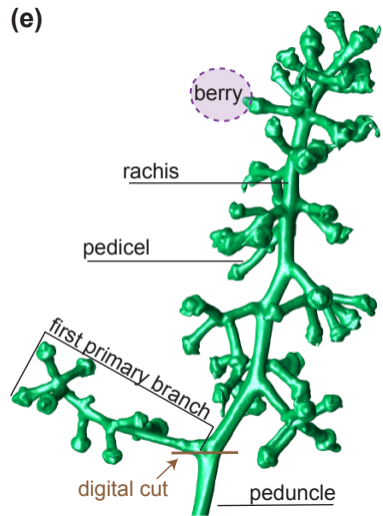
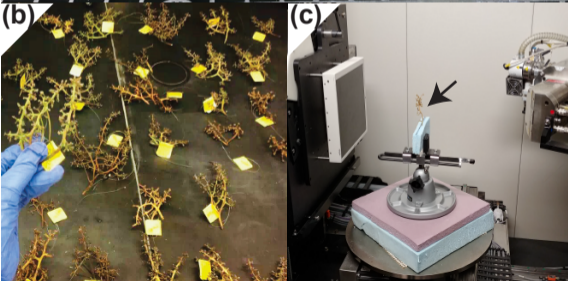
986

987 **Fig. 6** Classification for ten *Vitis* species based on inflorescence architecture. (a) Left:
988 Principal component analysis (PCA) plot on 24 morphological traits. The percent variance
989 for each PC explained is shown in parentheses. Species are shown in different colors. Right:
990 The loadings for the traits that contribute to the variance are shown. (b) Left: Linear
991 discriminant analysis (LDA) plot on the first 18 PCs (99.5% variance). Species are shown in
992 different colors. The confusion matrix for predicted species is shown in the upper right
993 corner. Right: The loadings for the traits that best distinguish species from each other are
994 shown. Using a jackknifed 'leave one out' cross validation, we obtain a 78.32% classification
995 accuracy rate.

996

997 **Fig. 7** Phylogenetic analysis. A Neighbor Joining phylogenetic tree for a subset of the *Vitis*
998 data set ($n=99$). Node values denote bootstrap support for values greater than or equal to
999 50. Ten *Vitis* species are highlighted in different colored backgrounds. Three clades (Asian
1000 Clade, NA Clade I, and NA Clade II) are labeled and marked by vertical bars. The barplot
1001 showing values of Pagel's lambda, an estimate of phylogenetic signal, overlaps with the
1002 trait name on the right top panel. Below each trait, a rainbow colormap shows the values
1003 for individuals (small values in red to large values in blue). Rectangles surround the trait
1004 value map for species with more than five individuals. One trait (PHn_PC1) was randomly
1005 selected to be projected onto the phylogenetic tree branches, and indicates trait variation
1006 (red, lower values; blue, higher values) within individuals and among clades.

1007



Geometric traits

global size features

Volume (mm³)

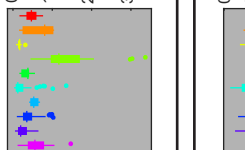
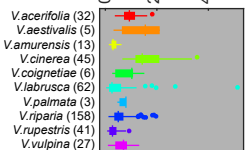
TotalBranchLength (mm)

121.95

251.5

827.38

1265.8



local branching features

RachisLength (mm)

PedicelBranchAngle (°)

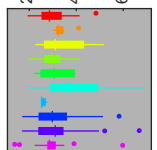
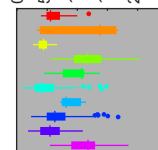
44.7

28.4

118.8

49.1

pedicel branch angle



size invariant features

Solidity

2nd/LongestBranch Length

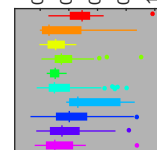
0.014

0.13

0.05

0.88

Longest
SecondLongest



Topological (persistent homology) traits

PersistentHomologyNormalizedByTotalBranchLength_PC1 (PHn_PC1)

PersistentHomology_PC1 (PH_PC1)

PersistentHomology_PC2 (PH_PC2)

-0.05

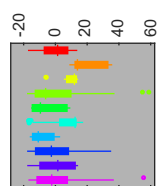
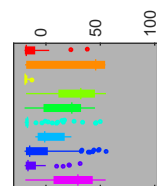
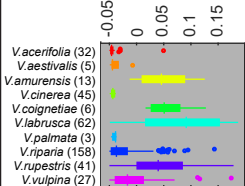
-19.65

-17.81

0.13

33.13

13.46



Berry potential traits

TotalBerryPotentialVolume (mm³)

AvgBerryPotentialDiameter (mm)

BerryPotentialTouchingDensity

4317.8

5.09

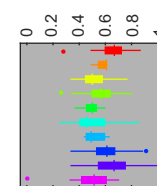
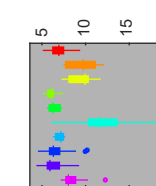
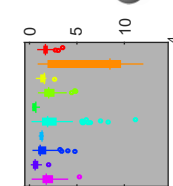
0

31476

11.74

1

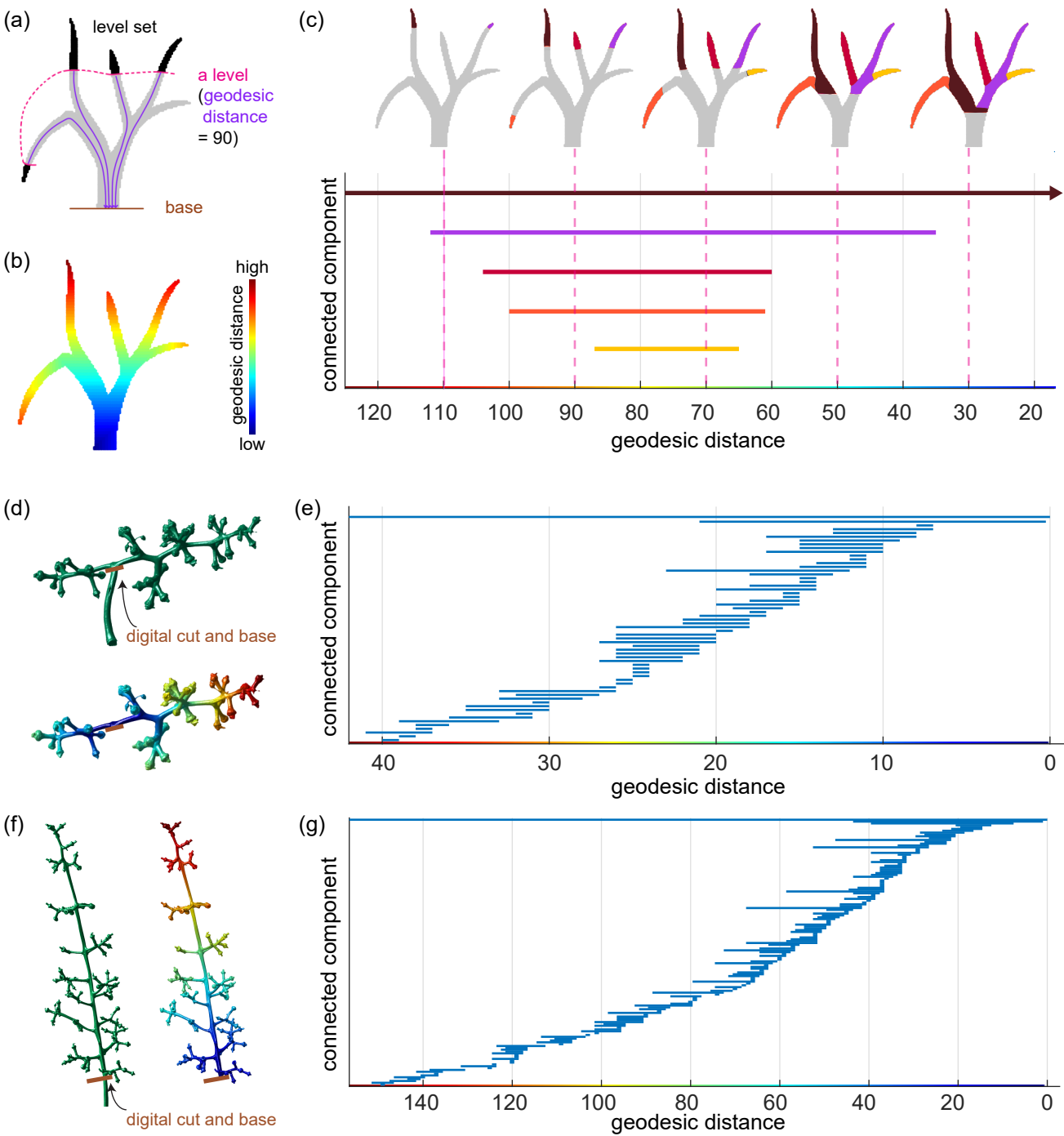
Berry Potential diameter

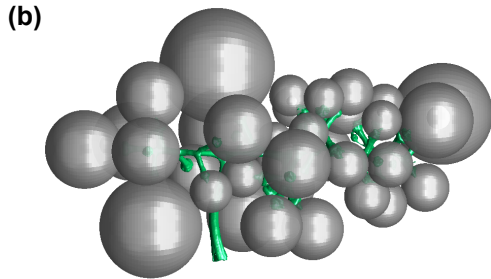
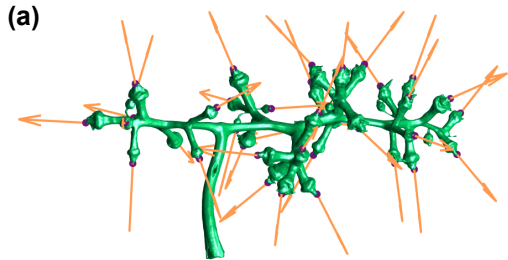


Distribution

Examples with low and high trait values

Distribution





STOP

- touches other berry potential

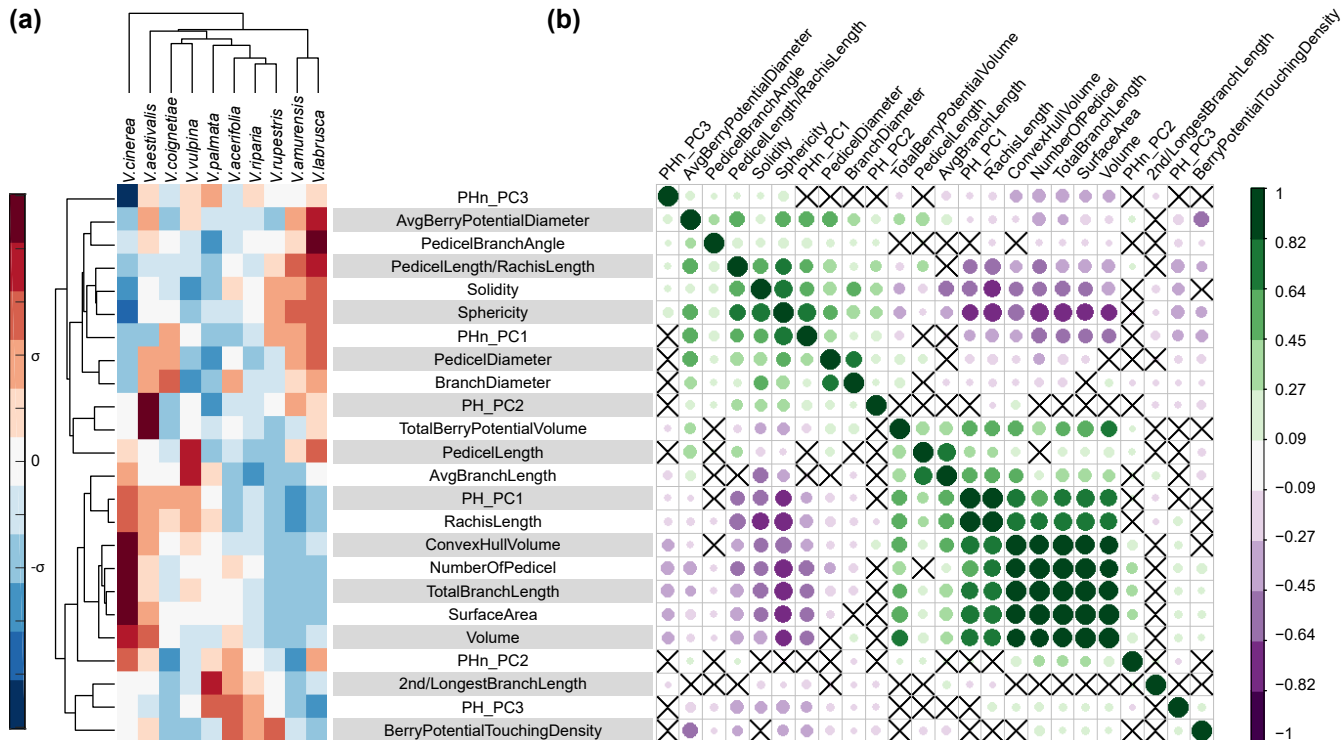


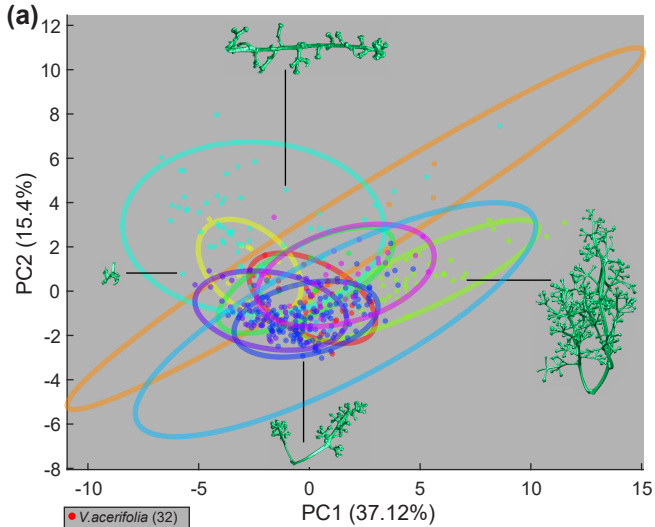
- touches branch



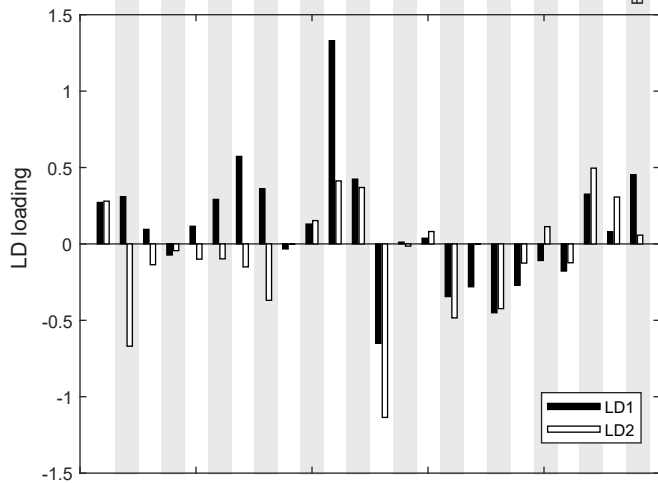
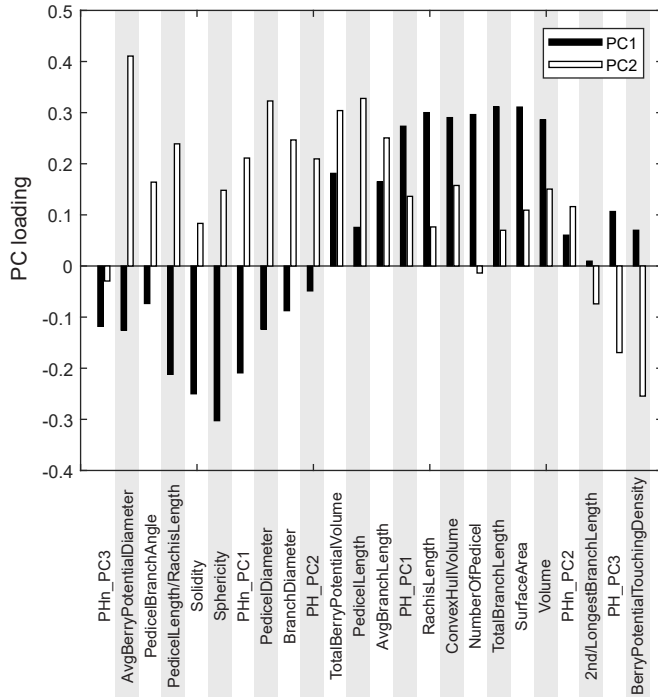
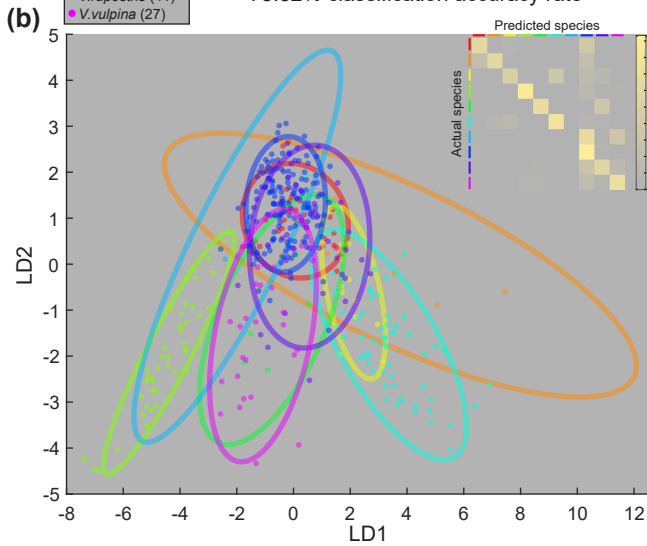
- reaches the size







78.32% classification accuracy rate



map each trait (e.g. PHn_PC1) onto the phylogeny

